Chinese Journal of Mechanical Engineering

ORIGINAL ARTICLE

Open Access

Simulation Analysis of Torsion Beam Hydroforming Based on the Fluid-Solid Coupling Method

Yu Huang, Jian Li*, Jiachun Yang, Yongdong Peng and Weixuan Zhang

Abstract

Hydroformed parts are widely used in industrial automotive parts because of their higher stiffness and fatigue strength and reduced weight relative to their corresponding cast and welded parts. This paper reports a hydraulic-forming experimental platform for rectangular tube fittings that was constructed to conduct an experiment on the hydraulic forming of rectangular tube fittings. A finite element model was established on the basis of the fluid–solid coupling method and simulation analysis. The correctness of the simulation analysis and the feasibility of the fluid–solid coupling method for hydraulic forming simulation analysis were verified by comparing the experimental results with the simulation results. On the basis of the simulation analysis of the hydraulic process of the torsion beam using the fluid–solid coupling method, a sliding mold suitable for the hydroforming of torsion beams was designed for its structural characteristics. The effects of fluid characteristics, shaping pressure, axial feed rate, and friction coefficient on the wall thicknesses of torsions beams during formation were investigated. Fluid movement speed was related to tube deformation. Shaping pressure had a significant effect on rounded corners and straight edges. The axial feed speed was increased, and the uneven distribution of wall thicknesses was effectively improved. Although the friction coefficient had a nonsignificant effect on the wall thickness of the ladder-shaped region, it had a significant influence on a large deformation of wall thickness in the V-shaped area. In this paper, a method of fluid-solid coupling simulation analysis and sliding die is proposed to study the high pressure forming law in torsion beam.

Keywords Fluid-solid coupling, Hydraulic expansion, Rectangular tube, Torsional beam, Wall thickness distribution

1 Introduction

Tube hydroforming is a hollow section metal forming process wherein a straight tube or a prebent blank is placed in a closed cavity, and a high-pressure liquid is injected to deform the tube to approximate the shape of the cavity and therefore obtain the intended cross-sectional shape. Researchers around the world have begun to analyze and study tube hydroforming given its advantages. Anaraki et al. examined the effect of pressure path on heat tube formability and wall thickness distribution [1–3]. Mirzaali et al. [4] used simulated annealing optimization method to study and optimize the pressure path during tube hydroforming. Ingarao et al. studied the variation of fluid pressure in the formation, which effectively improved the wall thickness thinning and the accuracy of fillet radius [5]. Yang et al. determined the effect of friction on the hydraulic forming accuracy of tube fittings under different loading paths [6]. Chen et al. used multiple linear regression analysis to discuss the influence of different parameters on the required liquid pressure [7]. Hao et al. proposed an improved axial feed hydraulic bulging process, and the results show that the strain of the improved bulging process is smaller than that of

*Correspondence:
Jian Li
lijian@gxust.edu.cn
Guangxi Key Laboratory of Automobile Components and Vehicle Technology, Guangxi University of Science and Technology, Liuzhou 545006, Guangxi, China

the conventional process [8]. Wei et al. designed and optimized prebulging parts based on response surface method. The results show that the forming performance is improved by the combination of the optimized prebulging and the hydraulic forming [9]. Ahmetoglu et al. verified the preforming of tubes and effectively improved the hydraulic forming limit of tubes [10]. Hashemi et al. developed a method for rapidly predicting the feasibility of the hydroforming process of concept parts. And they determined where failures or defects are likely to occur using enhanced unrolled inverse finite element methods and extended strain forming limit maps. Based on Kuczynski (M-K) theory, a fast method was developed to estimate the initial tube length, axial feed and fluid pressure during tube hydroforming. The results show that the finite element method can be used as a fast estimation tool for hydraulic forming process parameters of tube fittings [11].

In tube hydroforming, liquid is used as a force transfer medium to deform the tube under high pressure liquid. In the traditional numerical analysis of hydroforming, liquid supercharging is regarded as quasistatic. In the process of tube deformation, the liquid pressure acts on the inner wall of the tube as a uniform load, and the influence of liquid pressure change on tube deformation is ignored. Essentially, hydroforming is a complex fluid-solid interaction problem. Therefore, the fluid-solid coupling method is more accurate than the traditional method in numerical simulation analysis of hydroformed tube fittings. In fluid-solid coupling research, Li et al. used the fluid-solid coupling technology to simulate the whole physical process of bubble pulsation under the influence of gravity and verified the correctness of the finite element model [12]. Su et al. studied the interaction between tube deformation and fluid motion during hydraulic bulging of rectangular tubes by fluid-solid coupling method, and obtained the influence of flow field characteristics on forming performance [13]. Lee et al. simulated the flutter of the flexible plate in the fluid by fluid-solid coupling method [14]. Remigius uses coupling algorithms to couple interactions between Euler domains, making it possible to analyze complex fluid-solid interaction problems [15]. Rabczuk et al. studied the problem of high pressure and low speed body by fluid-solid interaction method, and simulated the fracture problem of cylindrical shell [16]. Ma et al. proposed a fluid-solid interaction algorithm to describe the dynamic behavior of fluid-solid interface, which accurately simulated the free surface flow of fluid, the deformation of elastic solid and the influence of fluid-solid interaction [17]. Therefore, the numerical simulation of tube fitting hydroforming based on fluid-solid coupling method can simulate the liquid pressure change and solid deformation under the actual flow field, and effectively reflect the interaction between liquid and tube fitting. The numerical simulation results have high authenticity and reliability. During tube hydroforming, the tube blank is filled with liquid (liquid) and pressurized to deform the tube (solid). The left and right punch and the inner hole form a coupling surface with the tube, and a virtual unit is arranged in the punch to determine the inflow conditions of liquid. The fluid-solid coupling forming method is different from the traditional hydroforming method, which realizes the real process of fluid inflow and pressure change. Therefore, it is of great value to use fluid-solid coupling to study tube hydroforming.

In this paper, the problem of torsional beam hydroforming based on fluid-solid coupling method was studied. Firstly, the hydraulic forming experiment platform of rectangular tube fitting was established, the hydraulic forming experiment of rectangular tube fitting was carried out, and the fluid-solid coupling finite element model of rectangular tube fitting hydraulic forming was established. By comparing the experimental results with the simulation results, the accuracy of the fluid-solid interaction numerical simulation method was verified, and the real variation of the fluid in the tube fitting was analyzed. On this basis, the finite element model of torsional beam hydroforming based on fluid-solid coupling method was established, and the preforming sliding mode of torsional beam was designed and the numerical simulation was carried out to study the flow characteristics of the fluid in the tube. In addition, the influence of forming pressure, loading path and friction coefficient on the wall thickness distribution was also studied.

2 Rectangular Tube Hydroforming Experiment

2.1 Experimental Platform Construction and Material Testing

Figure 1(a) is the schematic diagram of the experimental platform, and Figure 1(b) is the experimental platform. The experimental platform consists of hydroforming, pulsation generation, data acquisition and forming die. It can generate up to 70 MPa of hydraulic pressure and a maximum locking force of 600 kN.

The experimental push rod only plays the role of sealing, and there is no axial feed at the left and right ends. The sealing end is shown in Figure 2. The material is DC 03 steel and the sealing effect is enhanced by adding a high-pressure rubber sealing ring on the truncated cone. The physical picture of the mold is shown in Figure 3. It consists of an upper die and a lower die. The dimensions of rectangular tube forming die are shown in Figure 4. Considering that the rectangular tube die is symmetric, only the dimensions of the lower die are given. The straight edge of the bulging region is

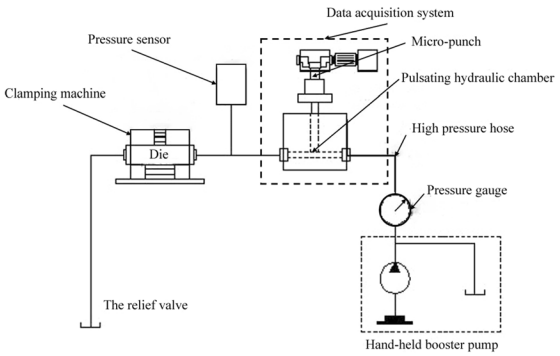

(a) Schematic diagram of rectangular tube hydroforming experiment platform

(b) Experimental platform for the hydroforming of rectangular: 1. Hand-held booster pump, 2.Pressure gauge, 3. Pulsating hydraulic chamber, 4. Micro-punch, 5.High-pressure hose, 6.Pressure sensor, 7. Pressure recorder, 8. Clamping machine, 9. Forming mold, 10. Pressure relief valve

Figure 1 Experimental platform for the hydroforming of rectangular tubes

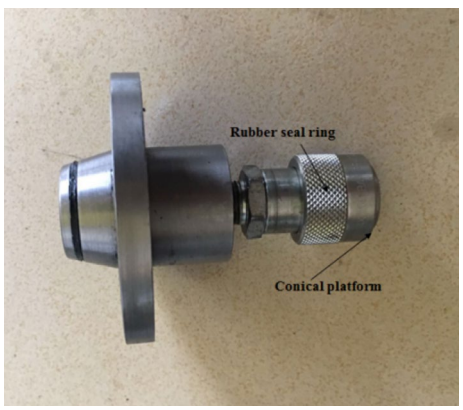

Figure 2 Sealing the end of the object

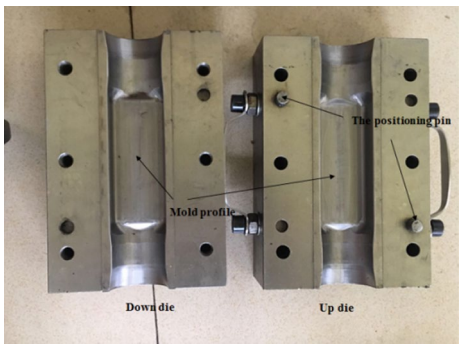

Figure 3 High-pressure forming mold in a rectangular tube

100 mm, the section length is 42 and 36 mm, and the fillet radius is 6 mm. The original tube was made of aluminum alloy tube with length of 175 mm, outer diameter of 40 mm and thickness of 1.9 mm, and the tube expansion ratio was 15.95%. The stress-strain curves and mechanical parameters of the experimental materials were obtained by uniaxial tensile tests. Tensile specimens are selected according to GB/T 228-2002 "Tensile Test Methods for Metallic Materials". The longitudinal bending sample of the tube fitting is shown in Figure 5. The size scheme of the specimen is shown in Figure 6. In this experiment, ETM105D microcomputer controlled electronic universal testing machine was used for tensile test, as shown in Figure 7. The drawing speed was 2 mm/s, the ambient temperature was standard room temperature, and the extender length was 50 mm. The sample after tensile test is shown in Figure 8. The fracture position of the sample is within the range of the original standard distance, and the tensile test results are valid.

Engineering stress s and engineering strain e are calculated as the average of the total length of the material. When the material enters the plastic phase, the cross-sectional size and length of the sample change, and the engineering stress and strain cannot truly reflect the mechanical properties of the material. In the process of tube hydroforming, the forming of tube mainly depends on the plastic deformation of material, and the mechanical properties of material must be characterized by the true stress σ and the true strain ε. According to the experimental stress-strain curve calculated from the experimental results, the true stress-strain curve of 6063-T6 aluminum alloy used in the experiment was calculated by using Eqs. (1) and (2), as shown in Figure 9.

$$\sigma = s(1+e), \tag{1}$$

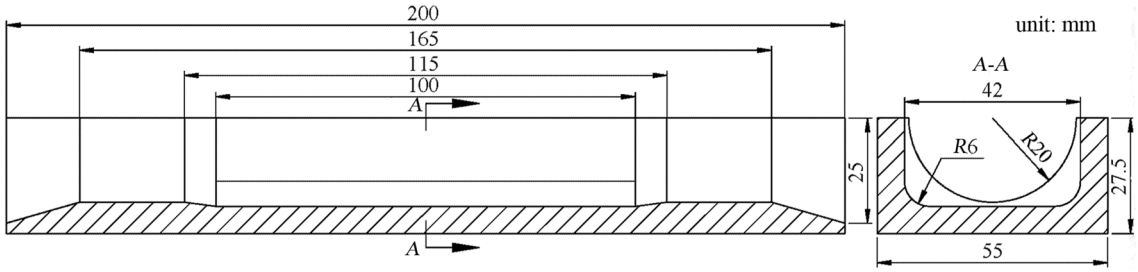

Figure 4 Dimensions of the rectangular tube forming die

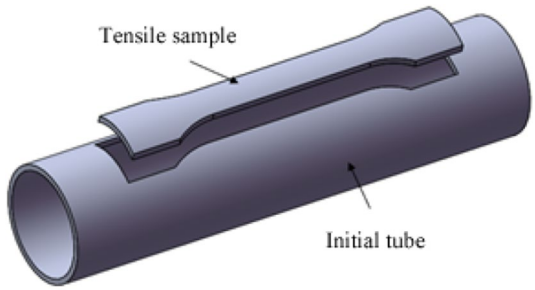

Figure 5 Schematic of tensile test cutting

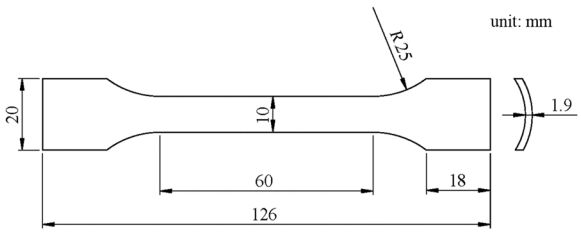

Figure 6 Tensile specimen size

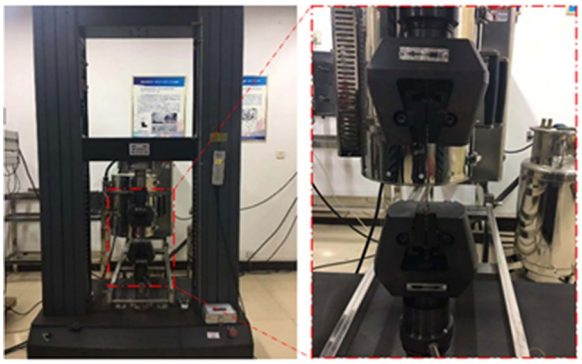

Figure 7 Stretching equipment and experiment

(a) Sample before stretching

(b) Sample after stretching

Figure 8 Tensile test specimen

$$\varepsilon = \ln(1+e). \tag{2}$$

Key parameters such as tensile strength σ_b, yield strength σ_s and elastic modulus E can be obtained from the true stress-strain curve, as shown in Table 1.

2.2 Hydraulic Bulging Experiment

Hydroforming experiments are carried out by increasing the liquid pressure to $P = 40$, 45, 50 and 55 MPa. The four forming results are shown in Figure 10. As shown in the figure, when the internal pressure $P = 40$ MPa, the horizontal and vertical right angles of the tube have been partially fitted, but the radius of the rounded corners of the tube is large, which does not achieve the desired effect. When the internal pressure $P = 45$ MPa, the clamping pressure of the mold increases to 40 MPa, but the filling effect of the rounded corners is still not good. When the internal pressure $P = 50$ MPa, the right angle edges of the four directions are almost all attached, and there is a clear right angle with the surface of the tube, the radius of the rounded corner decreases. When the internal pressure $P = 55$ MPa, the forming quality is the same as that when the internal pressure is 50 MPa. No changes are detected and the tube is no longer deformed at this time. The experimental results show that the internal pressure

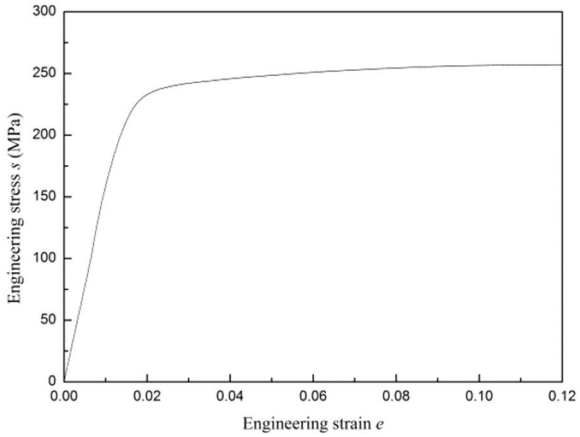

(a) Engineering stress–strain curve

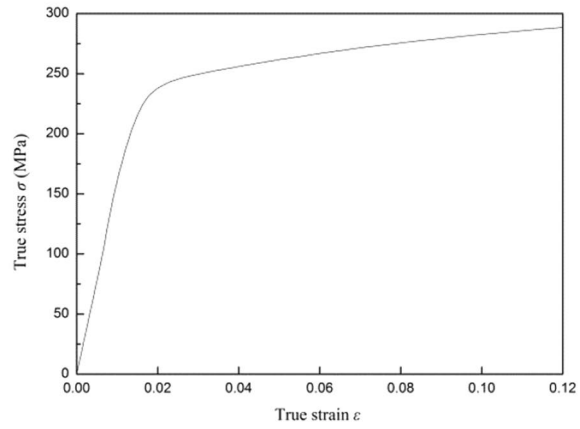

(b) True stress–strain curve

Figure 9 Stress-strain curve of the 6063–T6 aluminum alloy tube

required for the hydroforming of rectangular tubes decreases with the increase of the radius of fillet and increases with the increase of the length of horizontal and vertical right angles. Through theoretical formulas and experiment, we know that the fillet changes dramatically at 40–50 MPa, and the gap between the tube and the die decreases. Finally, the mold is completely rounded.

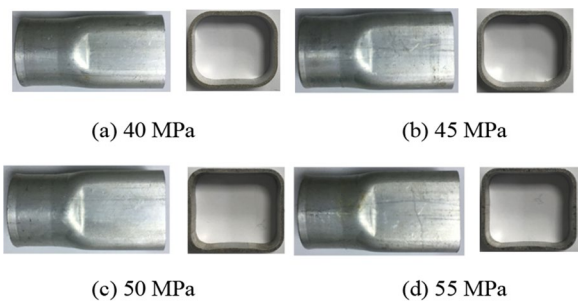

(a) 40 MPa (b) 45 MPa

(c) 50 MPa (d) 55 MPa

Figure 10 Forming results under different internal pressures

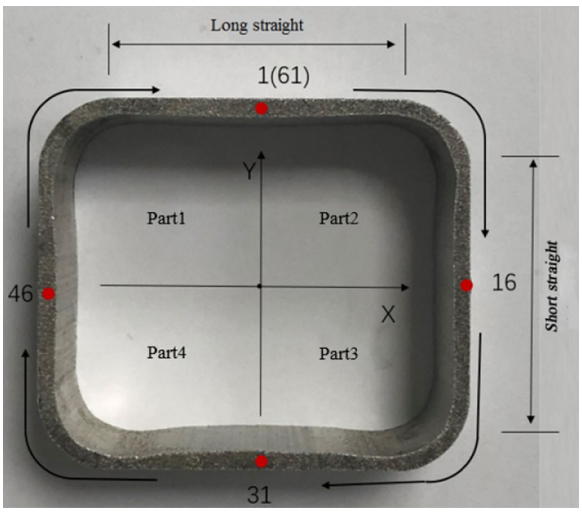

Figure 11 Distribution of the circumferential section of the intermediate section

When the pressure increases to 55 MPa, the radius of the fillet does not change much, and the deformed part of the tube does not expand with the increase of the internal pressure.

In order to further study the wall thickness distribution of the hydroformed rectangular tube under different internal pressures, the middle parts of the formed parts under the above four different pressures were selected and measured with vernier caliper. The rectangular tube section is symmetrical at the approximate coordinate axis, but it is divided into four parts because the straight side length and rounded corner radius of the forming results are different under different internal pressures, and 15 measuring points are evenly distributed in each part in the clockwise direction. A total of 60 measuring points are shown in Figure 11. The thickness of the measured point wall is shown in Figure 12. It can be seen from the figure that the wall thickness distribution of the forming parts is the same under different pressures. The wall thickness value is located at the midpoint of the long straight edge of each part. In addition, the wall thickness from the midpoint of the straight edge to the transition point gradually decreases, the wall thickness from the transition point to the center of the rounded corner increases, and the wall thickness at the rounded corner

Table 1 Parameters of the 6063-T6 aluminum alloy tube

Elastic modulus E(GPa)	Yield strength σ_s(MPa)	Tensile strength σ_b(MPa)	Poisson's ratio μ	Sclerosis index n	Elongation rate δ(%)
57	230.5	289.8	0.28	0.14	19.56

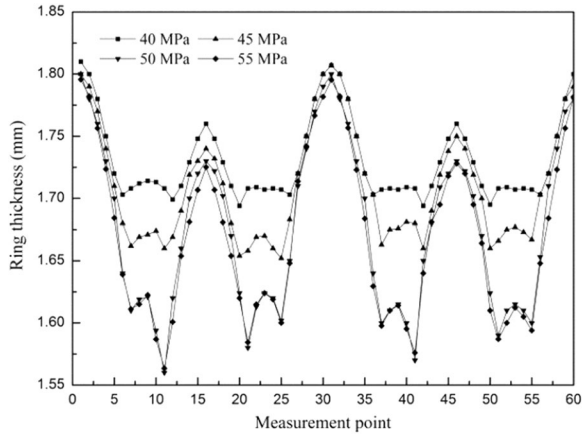

Figure 12 Distribution of the circumferential wall thickness of the intermediate section under different internal pressures

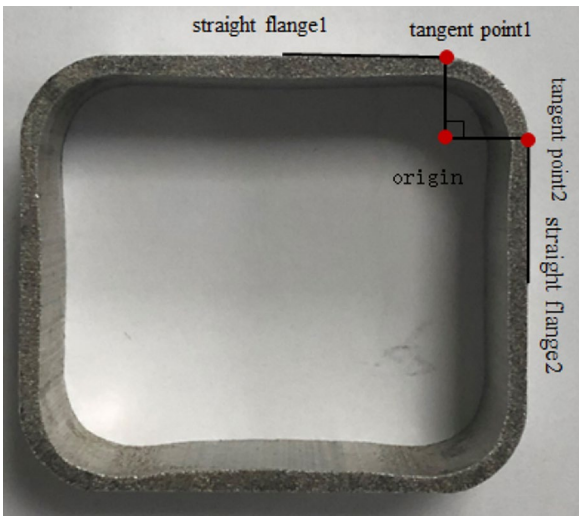

Figure 13 Fillet measurement mode

point is larger than that at the transition point. The wall thickness of the short straight edge part is similar to that of the long straight edge part, but the change of the former is more drastic than the latter, and the wall thickness of the transition area between the rounded corner and the straight edge area is the smallest in the whole circle. When the internal pressure increases from 50 to 55 MPa, the wall thickness of each part of the tube does not change. So at this point the tube is fully formed. After the rectangular tube is formed, the maximum wall thickness is located at the midpoint of the long straight edge. The maximum wall thickness is 1.81 mm. The minimum wall thickness is the transition area between the short straight edge and the rounded corner. The minimum wall thickness is 1.55 mm. The right fillet radius of the forming tube under different pressures was taken as the research object, and the fillet radius of four different pressure forming parts were measured, as shown in Figure 13. The cut points of long straight edge, short straight edge and rounded corner are taken respectively. The two cut points are taken as the vertical feet and make the vertical lines of the long straight edge and the short straight edge respectively. The intersection of these two perpendicular lines is the center of the circle, and the distance from the center to any point is the radius of the rounded corner. The measurement results of the fillet radius of the forming parts under different internal pressures are shown in Figure 14. When $P = 40$ MPa, the radius of the fillet is 10.10 mm. When $P = 45$ MPa, the radius of the fillet is 8.90 mm. When $P = 50$ MPa, the radius of the fillet is 6.00 mm. When the internal pressure is 55 MPa, the radius of the fillet does not change, which indicates that the tube fitting has been completely attached to the inner surface of the mold. When the internal pressure increased from 45 to 50 MPa, the radius of fillet increased faster than that when the internal pressure increased from 40 to 45 MPa. During the filling process, the internal pressure increases gradually with the decrease of the radius of the fillet.

3 Rectangular Tube Numerical Simulation

3.1 Finite Element Model

Based on the above experimental conditions, the high pressure forming process of rectangular tubes was numerically simulated by fluid-solid coupling method using MSC.DYTRAN nonlinear finite element software. The finite element model is shown in Figure 15. The model mainly includes Euler region, coupling surface, left and right punch, upper and lower die. In this paper, the hydraulic oil in the tube is defined as the Euler region,

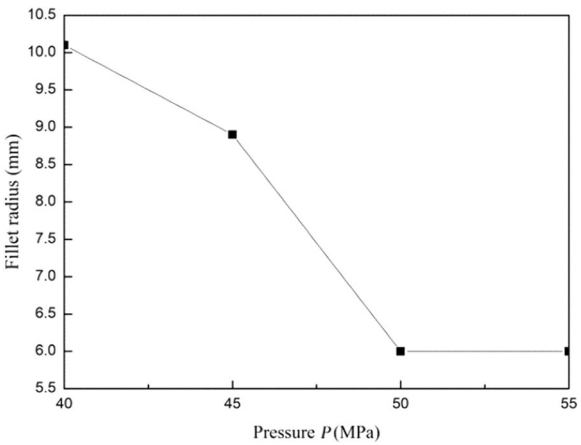

Figure 14 Fillet radius at different internal pressures

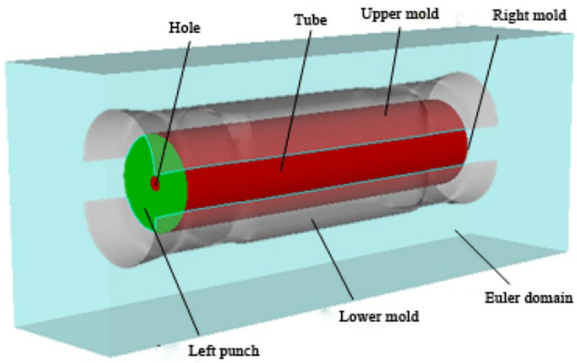

Figure 15 Geometric model based on the fluid–solid coupling method

which is a rectangle of 260 mm in length, 80 mm in width and 80 mm in height. The tube and die are located in the center of the Euler region. The model consists of an Euler grid, which is discretized into 8-node hexahedral elements, with a total of 24000 elements. Molds, push-rods, tubes, and other components are defined as Lagrange grids to establish rigid elements. A 4-node rigid shell element is used to discretize the upper and lower die, left and right push rods, tubes and virtual unit. The total number of units is 12732, as shown in Figure 16.

3.2 Comparison of Experimental and Numerical Simulation Results

Firstly, the friction coefficient between the actual die surface and the tube fitting is determined. The coefficient of friction is the only variable. In general, the friction coefficient of aluminum alloy material is 0.1–0.18. In order to ensure the accuracy of numerical calculation, the influence of friction coefficient on formation is studied. By comparing with the experimental results, the friction coefficients used in the numerical simulation are determined. Friction coefficient $\mu = 0.12, 0.14, 0.16, 0.18$. Under the condition that the final molding pressure is 55 MPa, the simulation analysis is carried out without axial feed. The wall thickness value is shown in Figure 17. The numerical simulation results are compared with the experimental results at $P = 55$ MPa. It can be seen from the figure that the wall thickness distribution is consistent when the friction coefficient $\mu = 0.16$ and the friction coefficient in the subsequent numerical simulation is 0.16.

In order to verify the accuracy of the fluid-solid coupling method and finite element model, the inlet pressure under four working conditions of 40, 45, 50, 55 MPa was simulated and analyzed according to the pressure linear loading mode. The wall thickness of the middle section of the forming tube under four different pressures is measured in Figure 18 and compared with the experimental results. As shown in the figure, the four groups of numerical results are consistent with the experimental results in terms of wall thickness distribution. When $P =$ 40 MPa (Figure 18(a)), the maximum wall thickness error is 3.21%. When $P = 45$ MPa (Figure 18(b)), the maximum wall thickness error is 4.12%. When $P = 50$ MPa (Figure 18(c)), the maximum error of wall thickness is 3.78%, and when $P = 55$ MPa (Figure 18(d)), the maximum error of wall thickness is 2.84%. The results of the four groups were compared. The experimental results show that the errors are within the controllable range, which not only verifies the correctness of the fluid-solid interaction method but also verifies the correctness and effectiveness of the finite element model.

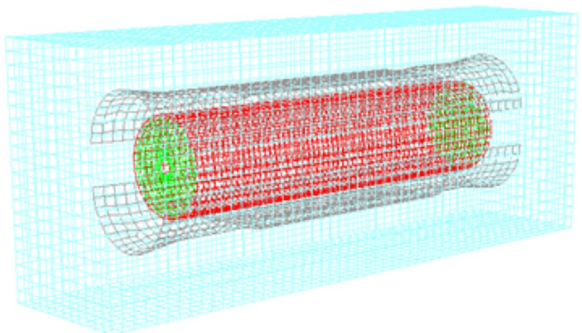

Figure 16 Finite element model based on the fluid–solid coupling method

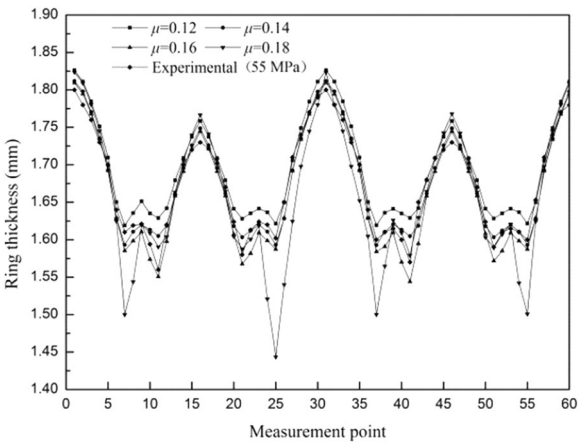

Figure 17 Comparison between the simulation results and experimental results for wall thickness

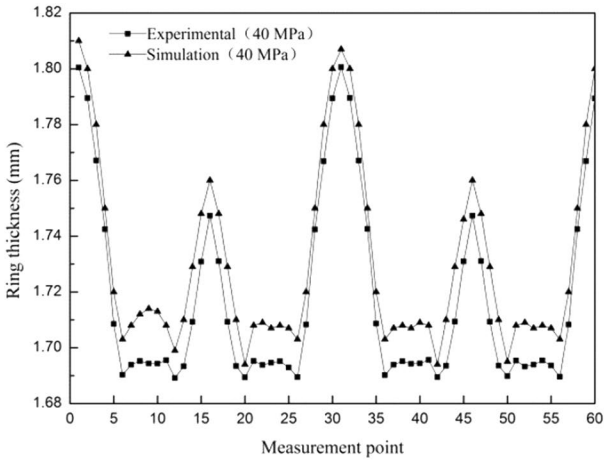

(a) Comparison of simulation and experimental results obtained under 40 MPa

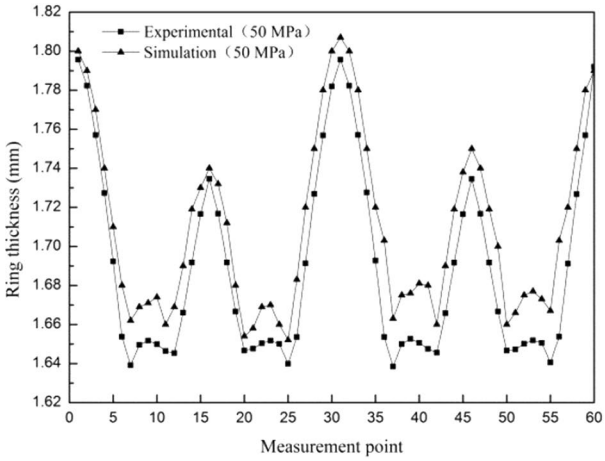

(c) Comparison of simulation and experimental results obtained under 50 MPa

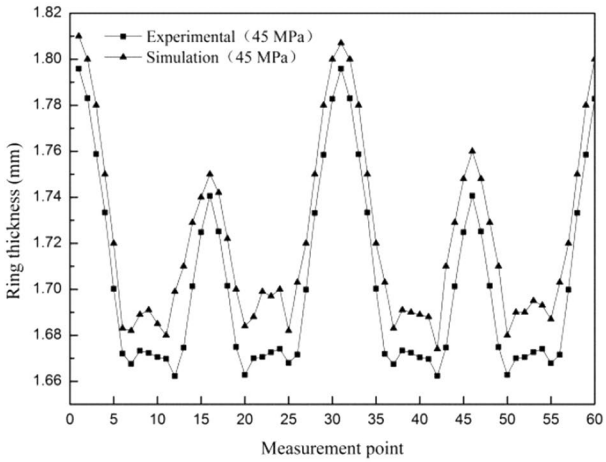

(b) Comparison of simulation and experimental results obtained under 45 MPa

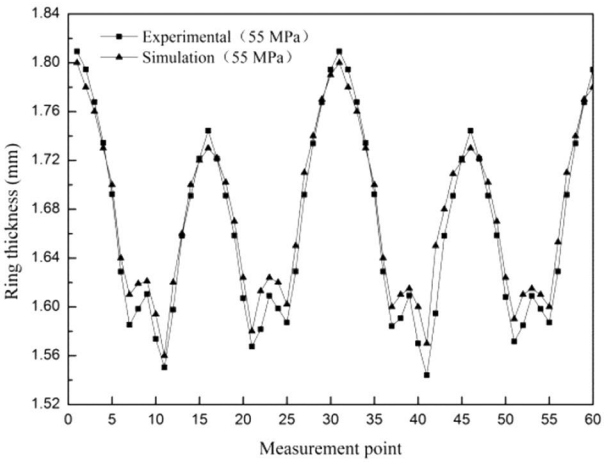

(d) Comparison of simulation and experimental results, obtained under 55 MPa

Figure 18 Comparison of simulation and experimental results obtained under different internal pressures

3.3 Analysis of Fluid Characteristics in the Tube

Considering that the volume of the tube fitting is not constant in the process of hydroforming, the flow velocity of the liquid injected into the tube fitting is different under the interaction between the pressure and volume of the tube fitting. As described in this section, the variation of liquid flow rate during tube fitting forming was studied at a final forming pressure of 55 MPa. As can be seen from the fluid velocity cloud of axial section in Figure 19, the fluid motion in the tube changes continuously, and the fluid velocity distribution in the tube is extremely uneven. The fluid inlet velocity on the left side is higher than that on the right side, and the fluid velocity shows a downward trend in the flow direction. Figure 20 provides a graph of the maximum fluid velocity variation during the forming process. As can be seen from the figure, the fluid velocity in the tube rises alternately, and the fluid velocity increases by two times. The first surge in fluid velocity occurs during the clamping phase when fluid is injected into the lumen and the increase in fluid velocity accelerates. After liquid filling is completed, the speed reduces and stabilizes at a reduced speed to continue liquid injection for pressurization. When the second injection velocity surge occurred at 0.17 s, the injected fluid velocity suddenly increased, and after the completion of injection, the fluid velocity decreased again and remained in a low range.

Figure 21 shows the maximum pressure change curve of the liquid in the rectangular tube. As can be seen from the figure, during the hydraulic process, the increase of

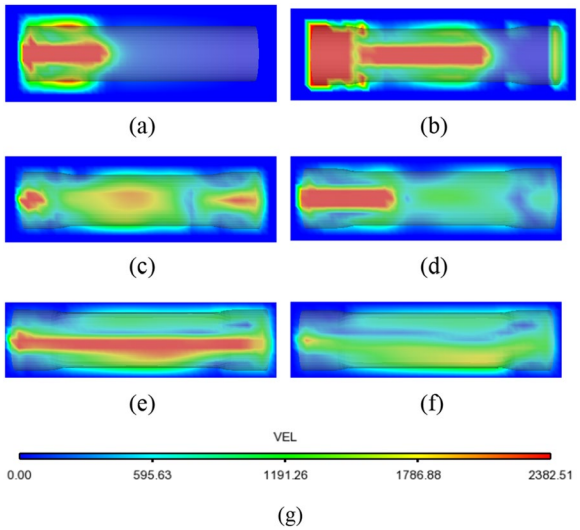

Figure 19 Cloud maps of fluid velocity in the axial section: (**a**) Cloud map of fluid velocity at 0.01 s, (**b**) Cloud map of fluid velocity at 0.02 s, (**c**) Cloud map of fluid velocity at 0.06 s, (**d**) Cloud map of fluid velocity at 0.12 s, (**e**) Cloud map of fluid velocity at 0.17 s, (**f**) 0.2 s fluid velocity cloud map, (**g**) Contour fluid velocity cloud map

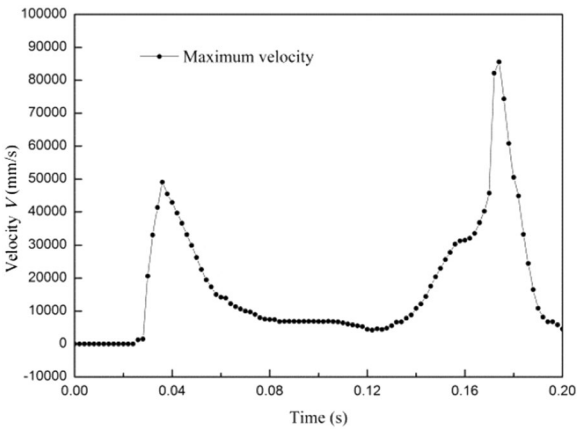

Figure 20 Maximum fluid velocity time history curve

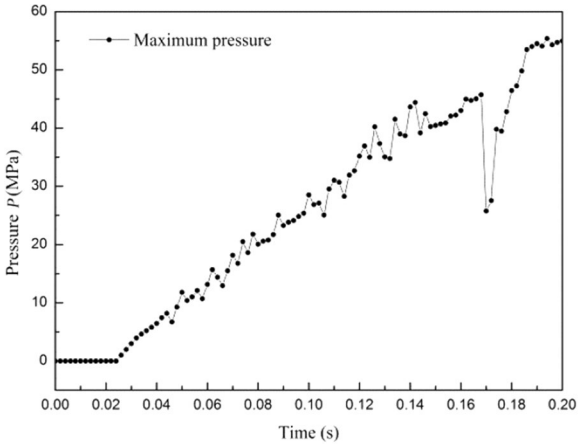

Figure 21 Time history curve of liquid pressure

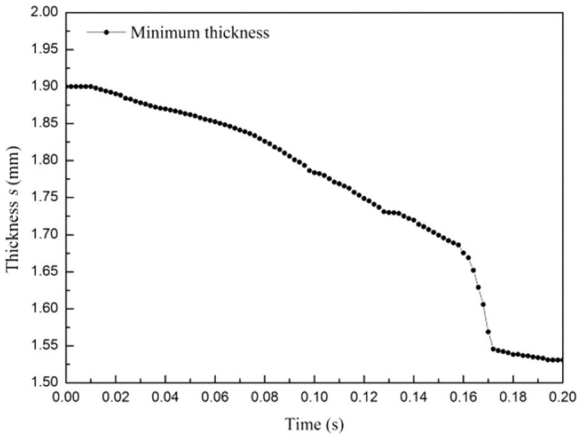

Figure 22 Time history curve of minimum wall thickness time history curve

the liquid pressure in the tube does not strictly follow the input target curve. However, when the pressure increases to a certain value, the internal volume changes suddenly. The wall thickness value drops sharply and the water pressure changes like irregular pulsation loading. When the internal pressure is 45 MPa, it drops to 25 MPa, and then with the rapid injection of liquid, the fluid velocity V surges, and the internal pressure rises rapidly and loads to the maximum target pressure. The recording curve of the minimum wall thickness of tube fitting forming is shown in Figure 22. The wall thickness decreases at a steady rate until the liquid pressure increases to 45 MPa. When the liquid pressure reaches 45 MPa, the tube wall thickness decreases sharply, from 1.60 to 1.54 mm. Subsequently, when the liquid pressure is pressurized to 50 MPa, the decrease rate of tube wall thickness slows down and tends to be stable. It can be seen from the figure that the sudden drop in liquid pressure when loaded to 45 MPa is caused by the sudden increase in volume change after the tube reaches a certain pressure. According to the relationship between pressure and volume in Crabone's equation, increasing the volume of the instantaneous lumen inevitably leads to a decrease in pressure. The velocity of the fluid in the tube rose sharply. When the pressure increased to 50 MPa, the wall thickness almost did not change, indicating that the tube was completely attached to the inner surface of the mold and the tube was formed.

4 Numerical Simulation of Torsion Beam Hydroforming Based on the Fluid–Solid Coupling Method

4.1 Torsion Beam Forming

In this section, the fluid-solid coupling method is used to analyze the torsional beam numerically. The mathematical model of the torsion beam is shown in Figure 23. The length of the forming zone of the torsion beam is 1240 mm, and there are feed zones of 30 mm on both sides, with a total length of 1300 mm. The expansion area of the torsion beam is mainly divided into three parts: the middle part of the "V" shaped area, the "concave" transition area and the "ladder" shaped end area. The remaining areas are transition zones and fill zones. The mold design and movement are shown in Figure 24. According to the characteristics of complex structure and large section deformation of torsional beam, two preforming processes were set up before hydraulic bulging. In Figure 24(a), the initial shape is first changed by the extrusion motion of the upper die, and then the width of the "V" shaped region decreases with the extrusion of the side die (Figure 24(b)), and finally the hydraulic bulging is performed (Figure 24(c)). The minimum section circumference of the torsion beam is taken as the standard. The tube fitting with external diameter of 46 mm, wall thickness of 3.5 mm and length of 1300 mm was selected as the initial tube fitting for high pressure forming of torsion beam. The material of the initial tube is SAPH440 high strength steel. The true stress-strain curve is shown in Figure 25. Material parameters are shown in Table 2.

4.2 Finite Element Model of Torsion Beam Hydroforming

Based on fluid-solid coupling method, the finite element model of torsional beam hydroforming was established. The solid composition is shown in Figure 26. The coupling surface is composed of tube blank, pusher 1, pusher 2 and liquid inlet, and the Euler domain is defined as the whole coupling surface. Euler and Lagrange grids use different types of discrete elements in numerical simulations. In Figure 27, the upper and lower die, left and right pusher head, tube blank, chuck 1 and 2, left and right sliding mode and virtual unit are discretized by 4-node shell element, and the number of units is 26232. Euler region is discretized by an 8-node hexahedral element with a number of 90000 elements. In this work, the upper and lower molds, left and right molds, fixtures 1 and 2 and left and right thrust heads are defined as rigid bodies. The blank is defined as a Lagrange unit. The contact

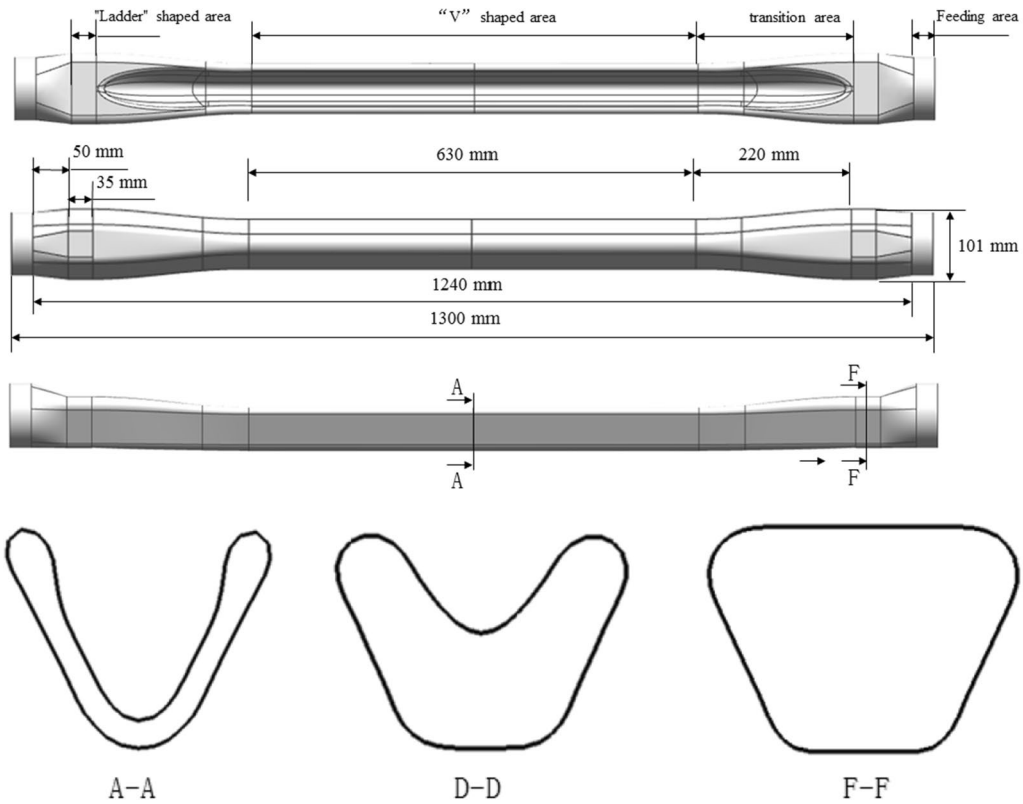

Figure 23 Mathematical model of the target torsion beam

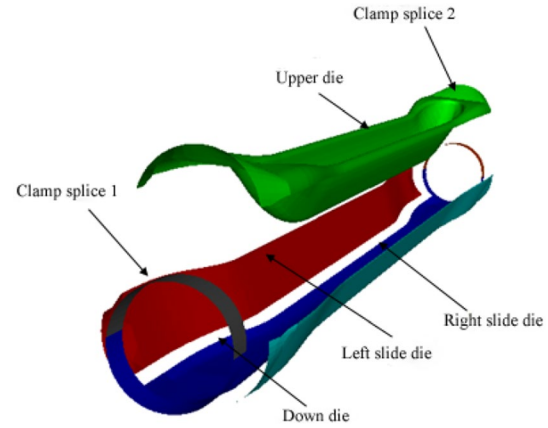

(a) The mold design

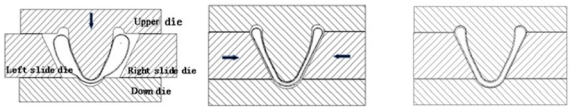

(b) Schematic of sliding mold movement: i) Upper die clamping, ii) Side extrusion of the left and right sliding die, iii) Hydraulic bulging

Figure 24 The mold design and movement

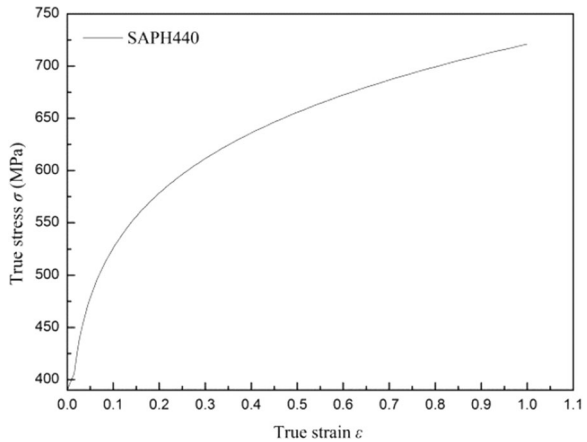

Figure 25 SAPH440 true stress-strain curve

between blank and die is defined as primary contact and secondary contact.

4.3 Numerical Simulation of Torsion Beam Hydroforming

In the process of hydraulic forming of torsion beam, the fluid in the tube interacts with the fluid in the forming tube, and the fluid movement in the tube is complex and irregular, which leads to the uneven distribution of tube wall thickness in the forming process. Torsion beam hydroforming can be divided into three stages: upper die closing stage, sliding die closing stage and hydraulic forming stage. Therefore, the effects of torsion beam on clamping, sliding clamping and hydraulic expansion are analyzed respectively. Figure 28 shows the wall thickness cloud diagram at each stage of the torsion beam, and Figure 29 shows the end thickness cloud diagram at each stage of the A-A, D-D and F-F sections. After the clamping stage of the upper die (Figure 28 (a)), the tube has the appearance of a torsional beam. It can be seen from Figure 29(a) that the "step" transition zone and the transition zone have sunk, leading to an increase in thickness. The maximum thickness δ_{max} is 4.36 mm. The V-shaped zone, inner and outer circle zone, and transition zone showed the most severe thinning. The minimum wall thickness δ_{min} is 3.29 mm, and the increase of wall thickness is more significant than the decrease of wall thickness at this stage. The maximum thickness thinning rate η is 6%. The slip-mode squeezes the sides of the tube. In Figure 28(b), the trapezoidal region is still wrinkled. The maximum wall thickness δ_{max} is increased to 4.58 mm, the minimum wall thickness δ_{min} is 3.30 mm, and the reduction ratio η is 5.71%. The inhomogeneity of wall thickness distribution is further increased. The hydroformed tube fitting is shown in Figure 28(c). Under the action of hydraulic pressure, the formed torsion beam has no fold, flattening completely and no cracking. The torsion beam shown in Figure 29(c) is under hydraulic pressure. The rounded corners have been pasted, and the minimum wall thickness has been transferred to the transition area on the straight side and the small rounded corners of the FF section. The minimum wall thickness δ_{min} was 2.76 mm, and the maximum thinning rate η was 21.24%.

Table 2 Parameters of the SAPH440 steel tube

Mass density ρ(kg/m^3)	Elastic modulus E(GPa)	Yield strength σ_s(MPa)	Tensile strength σ_b(MPa)	Poisson's ratio μ	Coefficient of hardening K(MPa)	Sclerosis index n	Elongation rate δ(%)
7830	198	390	606	0.28	776	0.19	32.8

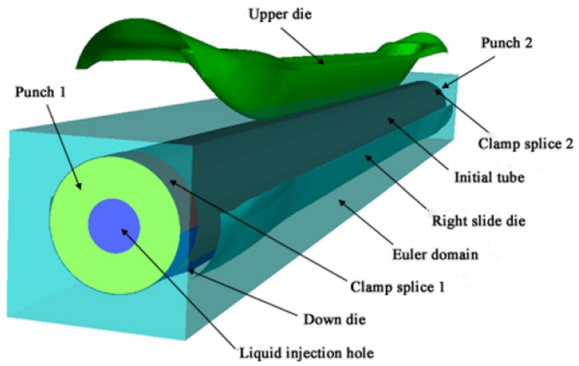

Figure 26 Flow–solid coupling model of high pressure

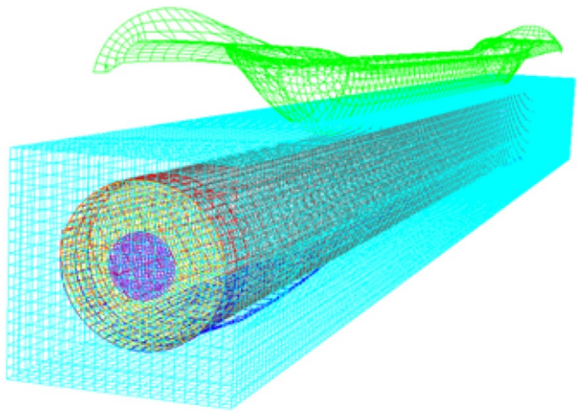

Figure 27 Finite element model mesh of discrete forming in torsion beam

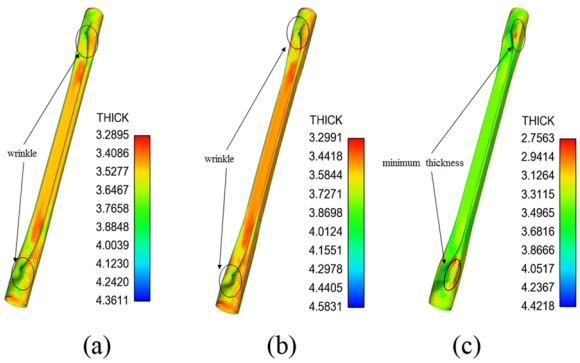

Figure 28 Cloud maps of thickness distribution at different stages: (**a**) Closing of upper mold clamping, (**b**) Closing of sliding mold clamping, (**c**) Closing of hydraulic bulging

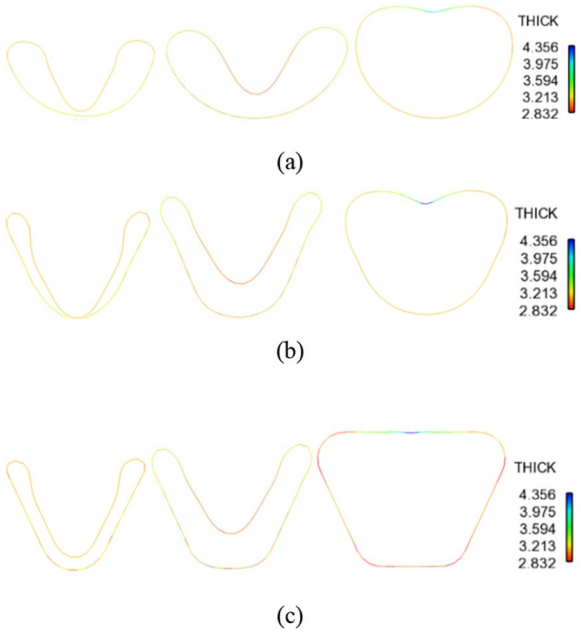

Figure 29 Cloud maps of the wall thickness of sections during torsion beam forming: (**a**) Cloud maps of the wall thickness of sections A–A, D–D, and F–F during the closing of the upper mold clamping, (**b**) Cloud maps of the wall thickness of sections A–A, D–D, and F–F during sliding mold clamping closing, (**c**) Cloud maps of the wall thickness of sections A–A, D–D, and F–F during the closing of the hydraulic bulging

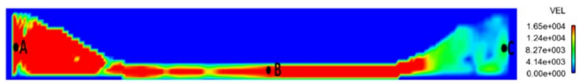

Figure 30 Distribution map of measurement points

5 Research the Forming Characteristics of the Torsion Beam Based on the Fluid–Solid Coupling Technology

In the process of hydraulic expansion of torsion beam, the change of flow field in the tube leads to the uneven change of pressure in the tube. Under the condition of initial liquid level of 30 mm and final forming pressure of 180 MPa, the axial plain profile of the fluid was dissected and analyzed. The plane is taken as the analysis object, and point *A* at the fluid inlet, point *B* at the midpoint, and point *C* furthest from the inlet are taken as the research object. Figure 30 analyzes the change of velocity *V* in the forming process and its internal influence rule.

It is complicated to evaluate the fluid velocity in the upper die closing, sliding die closing and hydroforming stages. Therefore, the fluid velocities at three different stages of torsional beam forming are selected for analysis. In Figure 31, the fitting deforms after the upper die is closed. Under the interaction between the tube fitting and

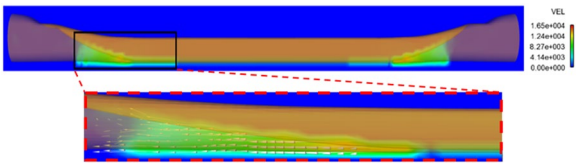

Figure 31 Cloud map of fluid velocity during upper die closing

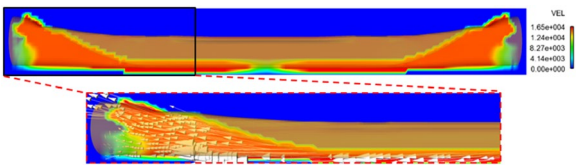

Figure 32 Cloud map of fluid velocity during sliding mold clamping closing

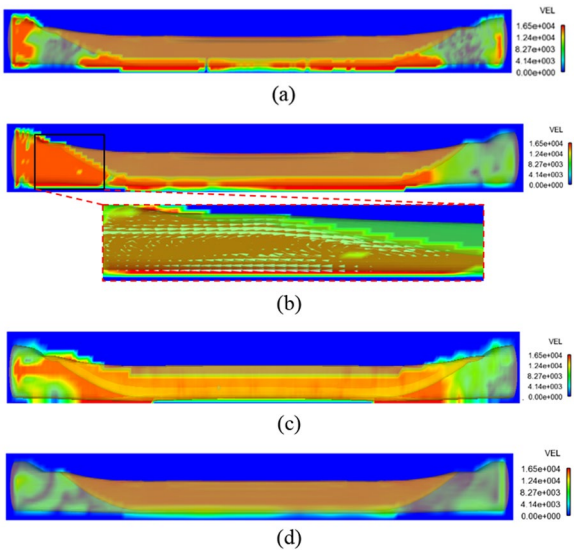

Figure 33 Cloud maps of fluid velocity during hydraulic bulging closing: (**a**) Cloud map of fluid velocity at 0.25 s, (**b**) Cloud map of fluid velocity at 0.28 s, (**c**) Cloud map of fluid velocity at 0.32 s, (**d**) Cloud map of fluid velocity at 0.40 s

the internal liquid, a small amount of fluid velocity is generated and transferred to both ends, and there is no fluid movement at both ends. In Figure 32, after the sliding mode compresses the side of the torsional beam, the fluid velocity increases sharply. At this point, the fluid velocity rises sharply to 1880.57 mm/s. The maximum velocity region is located at the bottom of both sides of the torsional beam, relative to the midpoint region. According to the fluid velocity cloud diagram in Figure 33, the fluid velocity in the tube does not increase uniformly. At 0.25 s, the inlet velocity of the left fluid gradually increased, the maximum peak velocity was 25341.60 mm/s, and the direction of the fluid velocity was parallel to the axial plane. The flow on the right side intersects with the fluid generated after the end of the sliding mode over time, and the fluid flow velocity in the torsional beam decreases between 0.25 and 0.28 s. As shown in Figure 33(c), the torsional beam is directly affected by the fluid motion on the trapezoidal section and the transition of the V-shaped section profile. Fluid motion is impeded from the side. The direction of the fluid velocity is switched to the right, generating a fluid vortex motion. At 0.29–0.32 s, the fluid velocity surges to 18016.98 mm/s. The fluid movement at the left inlet and outlet is more intense than in the middle region, and the fluid movement at the right side is slower than in the middle region. The liquid state tended to be stable between 0.33 and 0.40 s.

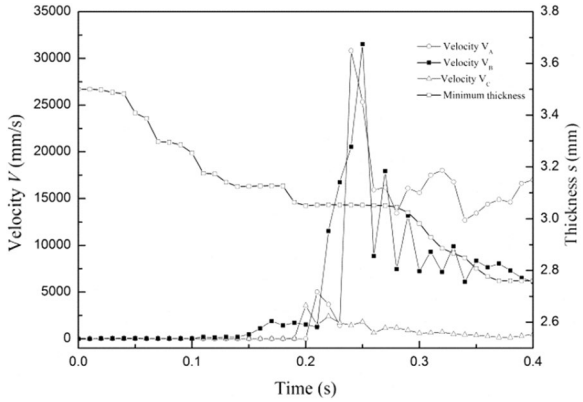

Figure 34 *A*, *B*, *C* three-point velocity and minimum wall thickness curve

The velocity V and the minimum wall thickness at points A, B and C are shown in Figure 34. As can be seen from the figure, the degree of fluid motion at point A is serious, and the degree of fluid motion at point B fluctuates and follows the motion at point A. The motion of point C is flat with no obvious fluctuations. The velocity V at point A has two peaks during expansion. The first peak velocities at points A, B and C are 0.24, 0.25 and 0.25 s, respectively. The second peak velocity at point A occurs at 0.32 s, and the next peak velocity at point B occurs at 0.33 s. When the peak value is reached, B and C are slower than A, and the velocity changes of A, B and C show a trend of fluctuation, indicating that the fluid in the tube flows from the left inlet to the other side, and finally shows fluctuation attenuation. When increasing to the second peak at point A, the minimum wall thickness of the tube decreases rapidly. After reaching the peak value, the steel tube deforms and the wall thickness decreases linearly. This behavior is accompanied by large

fluctuations in the velocity waveforms of *A* and *B*, and the drastic change in fluid velocity *V* indicates that the fluid velocity changes when the tube deforms during hydraulic bulging.

In the process of hydraulic expansion, the fluid velocity at the left inlet gradually increases, and the velocity direction is parallel to the axis. The fluid motion is hindered by the transition side of trapezoidal section and V-shaped section of torsional beam, and the velocity direction changes. When the fluid changes direction at high speed, it will increase the flushing force on the tube wall, so that the thickness of the tube wall will gradually decrease. Therefore, as shown in Figure 35, the left transition surface *D* and right transition surface *E* are taken as the research objects to analyze the changes of velocity *V* and wall thickness *S* in the bulging process. Figure 36 shows the variation curves of fluid velocity and wall thickness during the formation of *D* and *E*. As can be seen from the figure, the velocity at *D* sharply increases by 2 times during the hydraulic bulging process. The velocity and motion intensity of the fluid are significantly different from those at point *E*, where the fluid motion is gentle. From 0.28 to 0.40 s, the velocity of point *D* changes dramatically, and the thickness of point *D* and point *E* increases. Due to the strong fluid movement on the left side, the tube fittings bear a large load, which leads to an increase in the thinning degree of the wall thickness at point *D* compared with point *E*. The minimum wall thick-ness at point *D* is 2.99 mm, and the minimum wall thickness at point *E* is 3.12 mm.

6 Influence of Key Parameters on Forming Quality

6.1 Plastic Pressure

The effect of forming pressure on forming quality was studied, and the hydraulic pressure was linearly loaded to 140, 160, 180, and 200 MPa for analysis. The loading time was 0.18 s, and the friction coefficient between the tube fitting and the mold was 0.12. Figure 37 shows the distribution cloud of torsional beam wall thickness under different forming pressures. As can be seen from the figure, when the internal pressure reaches 140 MPa, the straight edge of the trapezoidal region of the torsion beam fits on the surface of the mold and is basically formed. However, the filling effect of the rounded corner area on the upper edge is not ideal. When the internal pressure is 160 MPa, the filling amount of transition zone and the rounded corner region of the torsional beam increases, and the

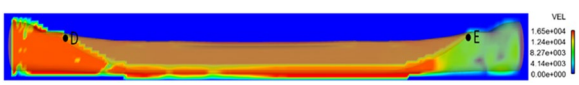

Figure 35 Distribution of fluid velocity measurement points at 0.28 s

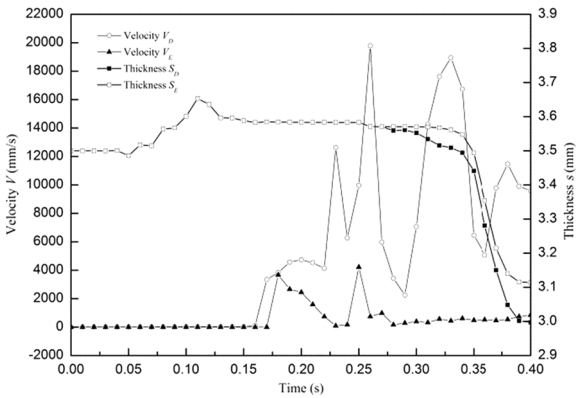

Figure 36 Curves of fluid velocity and wall thickness at points *D* and *E*

thinning region gradually concentrates on the transition region between the rounded corner and the straight edge. When the internal pressure exceeds 180 MPa, the wall thickness of the torsion beam is not affected by the forming pressure, indicating that the mold has stayed in its original position under the action of pressure.

The wall thickness distribution of each measuring point under different forming pressure and the variation of wall thickness between different forming pressure were analyzed. The wall thickness of each section was measured at 64 points in the F-F section. The F-F section with the largest wall thickness difference is taken as the research object, and the distribution of points is shown in Figure 38. The wall thickness distribution of F-F segment is shown in Figure 39. Under different forming pressure, the thickness distribution of the straight side wall is unchanged, but the thickness of the rounded corner is different from that of the straight side transition zone. In the range of 140–180 MPa, the thickness of the transition zone near the rounded corner and the straight side increases. When the internal pressure is 180 and 200 MPa, the wall thickness is 2.76 and 2.74 mm, respectively. The wall thickness distribution of the two is basically the

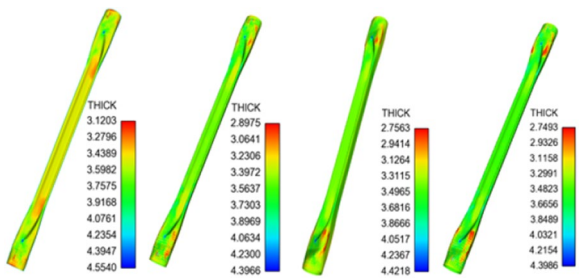

Figure 37 Cloud maps of thickness distributions under different plastic pressures

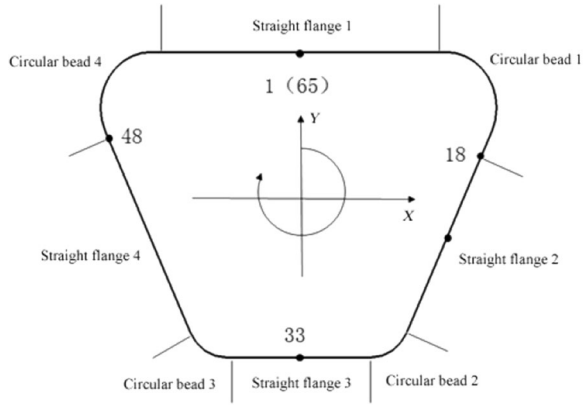

Figure 38 Schematic of the distribution of measurement points

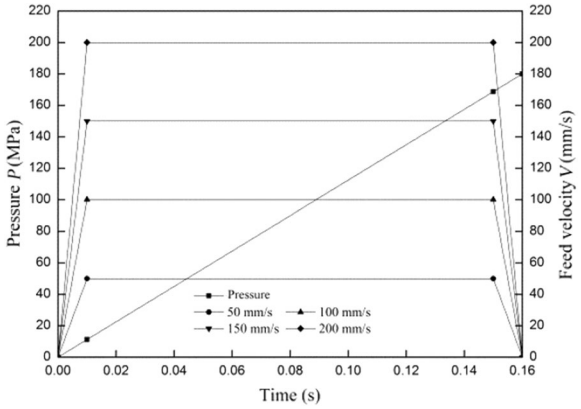

Figure 40 Load path with axial feed

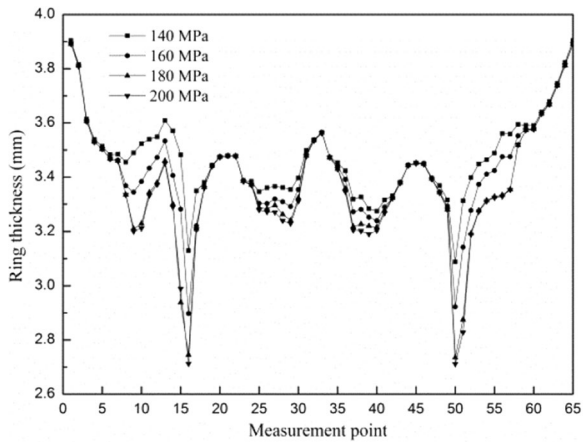

Figure 39 Wall thickness distribution of the F–F cross section

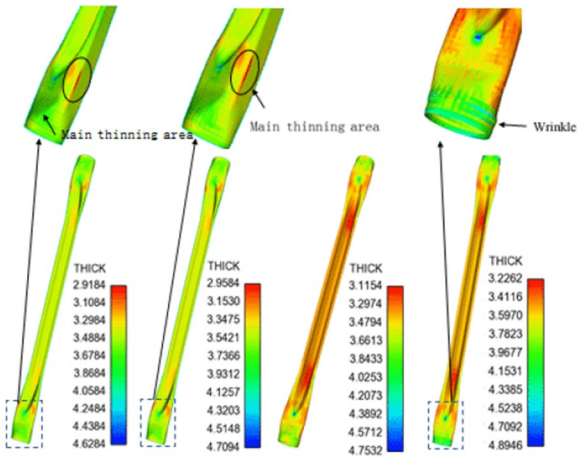

Figure 41 Cloud maps of the distribution distribution of the wall thicknesses of torsion beam

same, indicating that when the forming pressure of the torsional beam exceeds 180 MPa, the F-F section has been coated.

6.2 Loading Path

The minimum wall thickness of the torsion beam after hydroforming is located in the trapezoidal region, which is 2.76 mm, and the thinning rate is 21.14%. The area is in danger of breaking up. The effects of the feed rates of 50, 100, 150 and 200 mm/s on the quality of the forming parts were studied with the left and right axial feed rates as the research object. The loading path is shown in Figure 40. Figure 41 shows the wall thickness distribution of torsional beam at different feed speeds. When the feed speed increases from 50 to 150 mm/s, the minimum and maximum wall thicknesses of the torsional beam increase simultaneously. When the feed rates are 50 and 100 mm/s, the wall thinning is concentrated in the transition region between the small rounded corner and the straight edge of the trapezoidal zone. When the feed speed is 150 mm/s, the minimum wall thickness is located near the inside of the V-shaped zone and the transition zone, and the minimum wall thickness increases. When the feed speed is 200 mm/s, the end is wrinkled and cannot be flattened in the late pressure process. The results show that the forming quality is better when the feed speed is 150 mm/s and the minimum wall thickness $\delta_{\min}$ is 3.12 mm.

Figure 42 shows the curves of minimum wall thickness, maximum wall thickness, maximum thinning rate and maximum thickening rate under different coaxial feed speeds. It can be seen from the figure that with the increase of axial feed speed, the minimum wall thickness, maximum wall thickness and maximum thickness increase ratio of torsional beam all show an upward trend. The maximum thinning rate decreases with the increase of feed speed. Without axial feed, the minimum

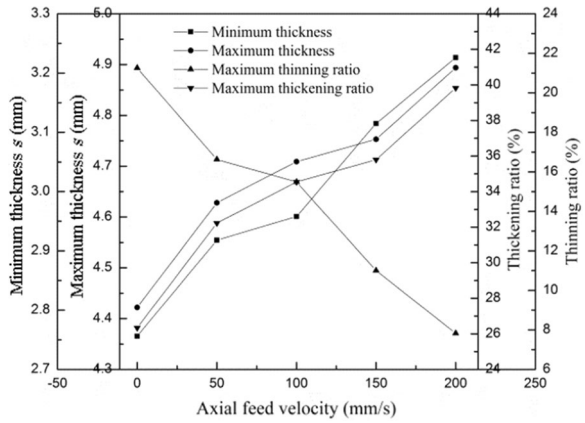

Figure 42 Minimum wall thickness, maximum wall thickness maximum thinning rate, and maximum thickening rate

wall thickness $\delta_{\min}$ increases from 2.76 to 3.12 mm, and the maximum thinning rate η decreases from 21.14% to 7.71%. Figure 42 is the curve of minimum wall thickness, maximum wall thickness, maximum thinning rate and maximum thickening rate under different coaxial feed speeds. It can be seen from the figure that with the increase of axial feed speed, the minimum wall thickness, maximum wall thickness and maximum thickness increase ratio of torsional beam all show an upward trend. The maximum thinning rate decreases with the increase of feed speed. Without axial feed, the minimum wall thickness $\delta_{\min}$ increases from 2.76 mm to 3.12 mm, and the maximum thinning rate η decreases from 21.14% to 7.71%.

6.3 Friction Coefficient

In the process of hydraulic forming of torsional beam, the tube fitting is in direct contact with the mold, the relative motion between the tube fitting and the mold is in dry friction state, and the friction coefficient is significant. If lead, lubricating oil and graphite are coated on the contact surface between the tube and the mold, the friction will be transformed into a mixed friction state of fluid friction, boundary friction and dry friction, which effectively reduces the friction coefficient and enhances the metal fluidity. The contact surface between the mold and the tube fitting is coated with soft metal lead for solid lubrication, and the friction coefficient is 0.08–0.2. The contact surface is lubricated with synthetic oil and the friction coefficient is 0.04–0.1. Therefore, the five friction coefficients μ of this section are 0.04, 0.08, 0.12, 0.16 and 0.2, respectively. The effect of non-friction coefficient on forming quality was studied under the conditions of axial feed speed of 150 mm/s and forming pressure of 180 MPa. The forming results of torsion beam under different friction coefficients are shown in Figure 43. With the increase of friction coefficient, the maximum wall thickness of torsion beam increases gradually, while the minimum wall thick-ness decreases gradually. When the friction coefficient is $\mu = 0.2$, the wall thickness of the transition zone between the straight side and the rounded corner of the V-shaped zone decreases sharply until the tube breaks.

Figure 44 shows the wall thickness distribution of F-F section under different friction coefficients. When the friction coefficients μ are 0.04 and 0.06, the wall thickness is low and uniform. When the friction coefficient continues to increase to 0.2, the wall thickness reaches the highest. The area affected by the friction coefficient is the transition area between round corner 1 and straight side 2, straight side 4 and round corner 4, because in the clamping stage, the round corner of the mold directly acts on the right side 2 and the right angle side. If friction increases, the flow of matter would be hindered. Therefore, the wall thickness is affected by the biaxial tensile stress and is severely thinned. Therefore, reducing the friction coefficient is beneficial to improve the

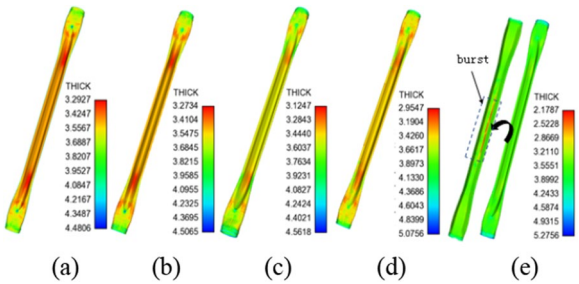

Figure 43 Cloud diagrams of the distribution of the wall thicknesses of torsion beams: (**a**) $\mu = 0.04$, (**b**) $\mu = 0.08$, (**c**) $\mu = 0.12$, (**d**) $\mu = 0.16$, (**e**) $\mu = 0.2$

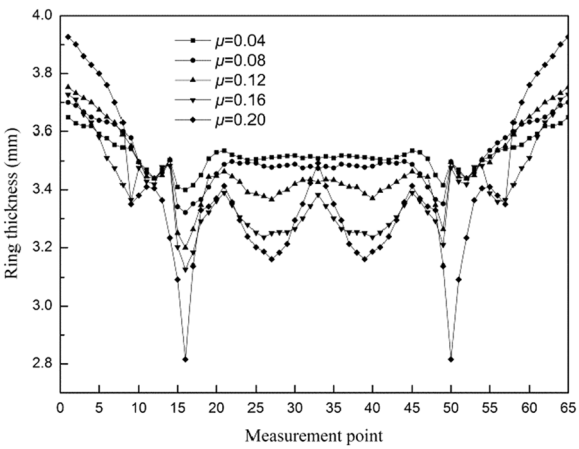

Figure 44 Wall thickness distribution the section F–F

friction between the tube and the die, so as to reduce the inhibition effect of the die on the tube material flow and increase the amount of material flowing into the rounded corner area.

7 Conclusions

In hydroforming, tube fitting deformation is a unidirectional fluid-solid coupling phenomenon of the interaction between fluid and tube fitting. On the basis of fluid-solid coupling method, the hydroforming of torsion beam is studied in this paper. Firstly, the rectangular tube hydro-forming platform is used to verify the correctness of the experimental and fluid-solid interaction simulation results. The hydroforming process of torsion beam was simulated by fluid-solid interaction method. The formation method of torsional beam and the flow in the tube are analyzed. The characteristics of the field and the influence of different key forming parameters on the forming effect were studied, which provided reference for the engineering application of tube fitting hydroforming. The specific conclusions are as follows.

(1) Comparing the wall thickness delta in the cross-section midpoint after the pressure of the hydraulic bulging experiment and the one after fluid-solid interaction through the numerical simulation for the rectangular tube under the forming pressures of 40, 45, 50 and 55 MPa reveals that the error of the simulation results is within 5%. The results verify the correctness of numerical simulation and finite element model. The characteristics of the flow field in the rectangular tube are analyzed. The results show that the liquid pressure in the tube varies unevenly, and the velocity difference in the tube is very significant, which is similar to the irregular pulse load. There are two sharp increases in the fluid velocity V in the tube. The sharp rise of the fluid is accompanied by a sudden drop of the tube pressure P and an acceleration of the wall thinning rate. These effects indicate that the internal hydraulic pressure P and fluid velocity V also change when the tube is suddenly replaced.

(2) The fluid-solid interaction of internal high pressure forming torsional beam is numerically simulated. At the end of clamping stage, the minimum wall thickness $\delta_{\min}$ is 3.29 mm, and the maximum thinning rate η is 6%. After the test, the minimum wall thickness $\delta_{\min}$ is 3.30 mm, and the maximum thinning rate η is 5.7%. The minimum wall thickness $\delta_{\min}$ is 2.76 mm, and the maximum thinning rate η is 21.24%. The analysis of the flow field inside the tube fitting during the forming process shows that when the liquid flows into one end of the tube fitting, the fluid velocity V at the inlet of the tube fitting and the middle of the tube fitting first increases and then decreases in a wavy shape. The further away from the inlet, the smaller the change in fluid velocity V, and the end with high velocity V is thinner than the end with low velocity V.

(3) The effect of fitting parameters on the forming quality of torsional beam was studied by fluid-solid coupling method. The severe thinning area is mainly concentrated in the transition point between the rounded corner and the straight edge. Increasing the axial feed velocity V is beneficial to improve the wall thickness uniformity and forming quality.

(4) With the increase of the friction coefficient, the maxi-mum thinning rate and the maximum thickening rate of the parts show an upward trend. When the friction coefficient $\mu = 0.2$, the minimum wall thickness of V-shaped region is 2.18 mm, and the thinning rate is 37.71%. Therefore, it can effectively reduce the friction coefficient, reduce the mold to tube flow obstruction, improve the quality of forming.

Acknowledgements
Not applicable.

Author contributions
YP, YH, and WZ designed the experimental work; YH and JY wrote the manuscript; JL was in charge of the whole trial. All authors read and approved the final manuscript.

Authors' Information
Yu Huang, born in 1994, received his M.S.degree in tube hydroforming from *Guangxi University of Science and Technology, China*, in 2020.
Jian Li, born in 1980, received his Ph.D.degree in general mechanics and fundamentals of mechanics from *Beijing Institute of Technology, China*, in 2009. He is currently a professor with *the School of Mechanical and Traffic Engineering, Guangxi University of Science and Technology, China.* His research interests include rehabilitation robot, automobile lightweight.
Jiachun Yang, born in 1994, received his B.S.degree in mechanical engineering from *Guangxi University of Science and Technology, China*, in 2020. He is currently pursuing the M.S.degree with *the School of Mechanical and Traffic Engineering, Guangxi University of Science and Technology, China*. His research interest includes tube hydroforming.
Yongdong Peng, born in 1992, received his M.S.degree in mechanical engineering from *Guangxi University of Science and Technology, China*, in 2019. His research interest includes tube hydroforming.
Weixuan Zhang, born in 1995, received his M.S.degree in mechanical engineering from *Guangxi University of Science and Technology, China*, in 2021. His research interest includes tube hydroforming.

Funding
Supported by Natural Science Foundation of China (Grant No. 81960332), Guangxi Provincial Innovation driven Development Project (Grant No. GKAA17204062), Guangxi Provincial Natural Science Foundation (Grant No. 2016GXNSFAA380211), and Liuzhou Municipal Scientific Research and Technology Development Plan (Grant No. 2016C050203).

Competing Interests
The authors declare no competing financial interests.

Received: 29 December 2021 Revised: 21 October 2022 Accepted: 31 October 2022
Published online: 05 January 2023

References

[1] A T Anaraki, L M Mohsen, L L Wang. Experimental and numerical investigation of the influence of pulsating pressure on hot tube gas forming using oscillating heating. *The International Journal of Advanced Manufacturing Technology*, 2018, 97(9-12): 3839-3848.
[2] F Dohmann, C Hartl. Hydroforming-A method to manufacture lightweight parts. *Journal of Materials Processing Technology*, 1996, 60(1-4): 669-676.
[3] J Jirousek, A Wroblewski. T-elements: State of the art and future trends. *Archives of Computational Methods in Engineering*, 1996, 3(4): 323-434.
[4] M Mirzaali, S M H Seyedkashi, G H Liaghat, et al. Application of simulated annealing method to pressure and force loading optimization in tube hydroforming process. *International Journal of Mechanical Sciences*, 2012, 55(1): 78-84.
[5] G Ingarao, R Di Lorenzo, F Micari. Internal pressure and counterpunch action design in Y-shaped tube hydroforming processes: A multi-objective optimisation approach. *Computers and Solids*, 2009, 87(9-10): 591-602.
[6] L F Yang, P Lei, C Guo. The influence of friction on forming accuracy of tubular parts by hydroforming with radial crushing. *Advanced Materials Research*, 2011, 328-330: 1386-1390.
[7] Y Z Chen, W Liu, Y C Xu, et al. Analysis and experiment on wrinkling suppression for hydroforming of curved surface shell. *International Journal of Mechanical Sciences*, 2015, 104: 112-125.
[8] Z Hao, S Luo, Z He, et al. Effect of plate hardening behavior on the deformation of stainless steel metal bellows. *Journal of Materials Engineering & Performance*, 2017, 26(1): 1-11.
[9] W Liu, Y Z Chen, Y C Xu, et al. Enhancement on plastic deformation of curved surface shell by sheet hydroforming with optimized pre-bulging process. *The International Journal of Advanced Manufacturing Technology*, 2018, 97(9-12): 4145-4156.
[10] M Ahmetoglu, T Altan. Tube hydroforming: state-of-the-art and future trends. *Journal of Materials Processing Technology*, 2000, 98(1): 25-33.
[11] R Hashemi, M B Shirin, M Einolghozati, et al. A different approach to estimate the process parameters in tube hydroforming. *International Journal of Material Forming*, 2015, 8(3): 355-366.
[12] J Li, J L Rong. Experimental and numerical investigation of the dynamic response of solids subjected to underwater explosion. *European Journal of Mechanics, B/Fluids*, 2012, 32: 59-69.
[13] H D Su, J Li, J L Rong, et al. Analysis of tubes with rectangular section forming process by fluid–solid coupling method. *The International Journal of Advanced Manufacturing Technology*, 2019, 102(5-8): 2491-2509.
[14] J Lee, J Shin, S Lee. Fluid–solid interaction of a flapping flexible plate in quiescent fluid. *Computers & Fluids*, 2012, 57: 124-137.
[15] W D Remigius, S Sunetra. *Fluid solid interaction of a flexible plate in a compressible medium*. New Delhi: Springer, 2017.
[16] T Rabczuk, R Gracie, J H Song, et al. Immersed particle method for fluid–solid interaction. *International Journal for Numerical Methods in Engineering*, 2010, 81(1): 48-71.
[17] X J Ma, M Geni, A F Jin. An algorithm for fluid–solid coupling based on SPH method and its preliminary verification. *International Journal of Computational Methods*, 2019, 16(2): 1846008.
[18] Z Yong, L C Chan, C G Wang, et al. Optimization for loading paths of tube hydroforming using a hybrid method. *Materials and Manufacturing Processes*, 2009, 24(6): 700-708.
[19] K T Lee, H J Back, H T Lim, et al. Tube hydroforming process design of torsion beam type rear suspension considering durability. *Interna-tional Journal of Modern Physics B*, 2009, 22(31-32):6199-6205.
[20] X Xu, S Li, W Zhang, et al. Analysis of thickness distribution of square-sectional hydroformed parts. *Journal of Materials Processing Technology*, 2009, 209(1): 158-164.